Volume 31 | Number 10 | October 2016 | Pages 1941–2102

JAAS

Journal of Analytical Atomic Spectrometry

www.rsc.org/jaas

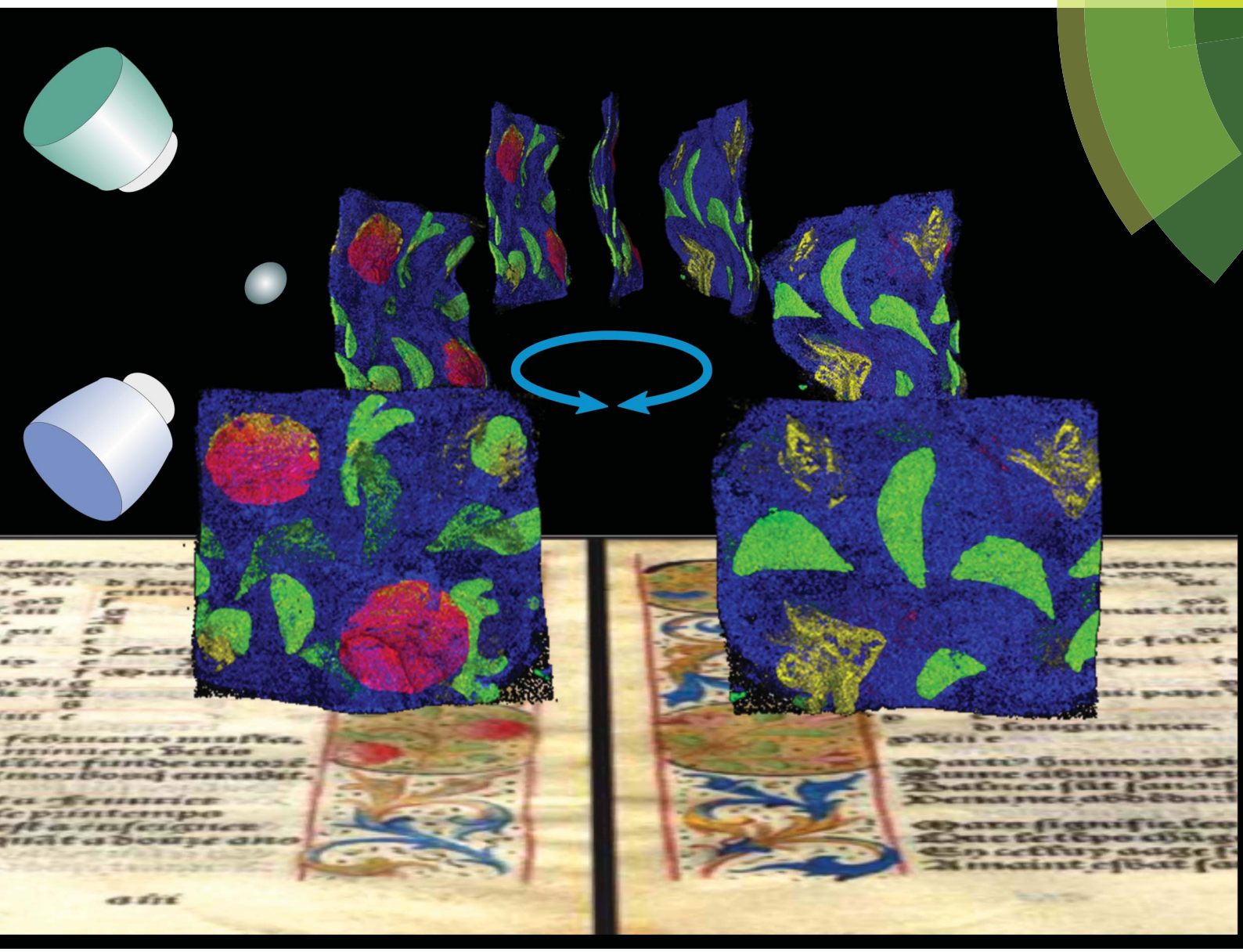

ISSN 0267-9477

ROYAL SOCIETY OF CHEMISTRY

PAPER

Ioanna Mantouvalou *et al.*

Combined 1D, 2D and 3D micro-XRF techniques for the analysis of illuminated manuscripts

175 YEARS

JAAS

PAPER

View Article Online
View Journal | View Issue

Cite this: J. Anal. At. Spectrom., 2016, 31, 1989

Combined 1D, 2D and 3D micro-XRF techniques for the analysis of illuminated manuscripts†

Tim Lachmann,[a] Geert van der Snickt,[b] Michael Haschke[c] and Ioanna Mantouvalou*[a]

Received 16th June 2016
Accepted 25th August 2016

DOI: 10.1039/c6ja00220j

www.rsc.org/jaas

The combination of several micro-XRF analysis modes is presented for the investigation of an illuminated parchment manuscript. With a commercial instrument, conventional micro-XRF spot analysis (0D) and mapping (2D) are performed, yielding detailed lateral elemental information. Depth resolution becomes accessible by mounting an additional polycapillary lens in front of an SDD detector. Quantitative confocal depth profiles (1D) are presented as well as the full separation of the front and the backside decorations with the help of fast 3D mappings of specific areas. Only through the use of these multi-dimensional modes can elemental information be assigned both to lateral and depth positions, making the analysis of such heterogeneous samples feasible.

1 Introduction

In the field of art and archaeometry, questions concerning manufacturing techniques or provenance often require the selective analysis and characterization of layers in stratified samples such as paintings, glasses, ceramics or decorated parchment.[1–3] Often, in such cases sampling is performed for the investigation of cross-sections with *e.g.* optical microscopy or SEM-EDX. Although sampling is called micro-invasive, it does invade the object and is, thus, not desirable or even impossible in some cases.[4]

X-ray fluorescence spectroscopy (XRF) is a non-destructive technique which delivers information about the qualitative and quantitative distribution of elements in one, two or even three dimensions. By using X-ray optics such as polycapillary lenses, the excitation radiation can be focused onto a small spot, rendering laterally resolved micro-XRF analysis possible.[5] The introduction of a second optic in the detection channel in a confocal geometry allows the additional generation of depth resolution through the formation of a localized probing volume.[6,7] In this way, the qualitative three-dimensional determination of elemental distributions of heterogeneous objects becomes feasible.

Through the knowledge about the interaction between X-rays and matter also quantitative information is accessible. With fundamental parameter algorithms based on the Sherman equation,[8] fluorescence information can be converted into mass depositions and in the case of confocal measurements, the elemental compositions and thicknesses of layers can be derived.[9,10]

One micro-XRF spectrum contains information about elements on one specific lateral spot without any depth resolution. The information depth for each element in a specific matrix is dependent on the fluorescence energy and, thus, element and fluorescence line specific. Assuming homogeneous layers and with additional knowledge about the sample, such as the number and sequence of layers and an initial guess of the composition, characterization of layers, *i.e.* the determination of their thickness and composition, becomes within reach.[11,12] However, the investigation of elemental depth gradients or samples where one element is present in consecutive layers often constitutes the limit of such an analysis.

When using confocal micro-XRF, fluorescence information is only detected from a localized probing volume, which can be moved in three dimensions through a sample. In particular for specimens with low attenuation, the sequence of layers can be made visible immediately. Nevertheless, the qualitative measured data must be interpreted with care due to absorption effects of superimposed materials and the energy-dependent nature of the formed probing volume. Until now, quantification models exist only for laterally homogeneous layers,[10,13,14] so that 3D mapping of heterogeneous samples remains qualitative even if an absorption correction is conducted.

In this work, we present the confocal analysis of an illuminated foil of parchment extracted from a 15th/16th century book of tides featuring scripture and decoration on both sides.[15] The materials were previously characterized using micro-XRF, micro-Raman spectroscopy and micro-XRD. This previous work led to a deeper understanding of the used pigments while highlighting the difficulty of assigning the ensuing (X-ray) information to the front or backside features on the parchment.

[a]Institute for Optics and Atomic Physics, Technical University of Berlin, D-10623 Berlin, Germany. E-mail: ioanna.mantouvalou@tu-berlin.de; Fax: +49 30 314 23018; Tel: +49 30 314 79057

[b]University of Antwerp, Department of Chemistry, AXES Group, Antwerp, Belgium

[c]BLiX – Berlin laboratory for innovative X-ray technologies, Berlin, Germany

† Electronic supplementary information (ESI) available: Animation of the 3D mapping of two selected regions. See DOI: 10.1039/c6ja00220j

For this reason, micro-XRF and confocal micro-XRF analyses were performed with the setup described below, leading to selective lateral and 3D visualization of elemental distributions on both sides of the foil, in selected regions of interest. Quantitative micro-XRF spot analysis and confocal micro-XRF depth profiling demonstrate the possibilities and limits of the analytical performance for highly heterogeneous objects.

2 Materials and methods

2.1 Experimental setup

The measurements were performed with a modified Bruker M4 Tornado. In the original configuration, this laboratory micro-XRF instrument is designed for ultra-fast 2D-measurements[16] using a micro-focus Rh tube in combination with a polycapillary optic and two SDD detectors. The X-ray tube with the optic and the two SDD detectors are arranged with a 50° angle to the sample surface. The sample stage is motor driven with a step size as small as 4 μm for all three dimensions. The data collection can be performed step by step or in an on-the-fly mode *i.e.* the stage is continuously moving during the measurement. The sample chamber can be evacuated to 20 mbar and an optical microscope with two magnification stages is utilized for positioning.

In this work, the instrument was modified in order to allow, besides two-, also three-dimensionally resolved measurements with the help of two X-ray optics in a confocal arrangement. For this purpose, a polycapillary was placed in front of one of the SDD detectors with an 80° angle between the excitation and detection channel. In this configuration both conventional micro-XRF and confocal micro-XRF can be performed sequentially with the same instrument.

The lateral resolution of the spectrometer was measured with a Fe knife edge sample and it amounts to 20 μm × 29 μm (90 : 10 criterion) at 6.4 keV. The depth resolution and the sensitivity as defined in ref. 13 are displayed in Fig. 1. All three parameters are functions of energy due to the used polycapillary optics. The FWHM of the probing volume in the depth direction

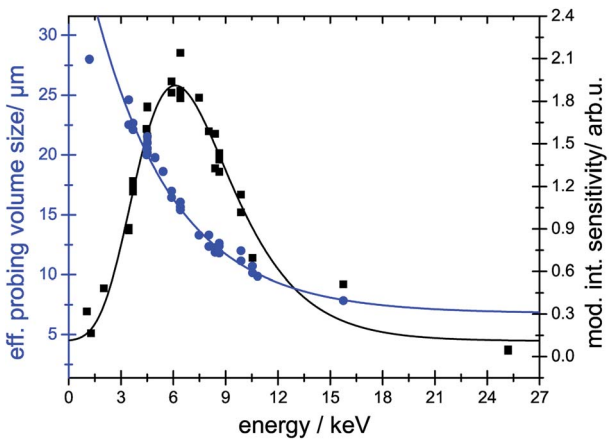

Fig. 1 Calibration of the probing volume; the depth resolution (blue circles and curve) and the sensitivity (black squares and curve) as defined in ref. 13 are functions of energy.

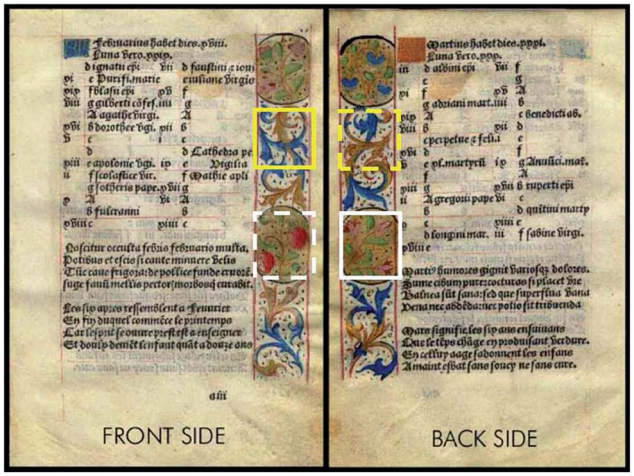

Fig. 2 Front and backside of the parchment sheet with indication of two mapping areas 'scrollwork' (yellow outline) and 'strawberry/flower' (white outline); the 'scrollwork' area was mapped with the 'front side' of the parchment facing the measuring head while the 'strawberry/flower' area was scanned from the 'backside' of the parchment, *i.e.* with the flower side facing the measuring head.

decreases from 60 μm at Sn L_α (3.444 keV) to 20 μm at Zr K_α (15.775 keV), while the sensitivity is highest for fluorescence energies between 4 keV and 9 keV.

2.2 Sample

Fig. 2 shows a photograph of the front and backside of the parchment with text in black ink, red-pink rulers and richly decorated gilded cartouches delineated with black contours. The materials were studied by means of combined micro-XRF, micro-Raman spectroscopy and micro-XRD in a previous work.[15]

Two areas of interest were selected (see Fig. 2): an area showing scrollwork on both sides of the foil ('scrollwork' area marked with yellow) and an area with gilded cartouches, one depicting strawberries (front side) and one showing flowers (backside) ('strawberry/flower' area marked with white). Both areas are of special interest for this study as the same pigments are present on both faces, complicating a full depth analysis from one side. In this work, we present the combination of micro-XRF point analysis (0D), micro-XRF mapping (2D), confocal micro-XRF 3D mapping (3D) and quantitative depth profiling (1D) for the investigation and separation of the decoration on both sides.

With the aim to achieve flatness on the micrometer scale, the sample was fixed on a steel plate with large area magnets. In order to avoid contributions from the plate to the measured signal, the sample was positioned over a void with a diameter of approximately 35 mm.

3 Experimental

All measurements were performed in air with an X-ray tube voltage of 50 kV and a current of 600 μA without a primary beam filter.

3.1 Micro-XRF measurements

A 2D micro-XRF measurement of the 'strawberry/flower' area was performed with the flowers oriented towards the detector, see Fig. 3. The top left picture is an optical image of the 'flower' area which was facing the detector for comparison with the elemental distributions. The other pictures are produced by summing over specific energy regions (regions-of-interest: ROI) for the respective fluorescence line. The analyzed area was approx. 22 × 26 mm^2 with a step size of 15 μm which results in 1613 × 1487 pixels (total 2.4 Mio). With a pixel time of 1 ms the total measurement time was approximately 70 min. For each pixel, the fluorescence spectrum is saved enabling a detailed analysis after the measurement. The count rates achieved with this arrangement lie in the range of 50 kcps *i.e.* for a short measurement time, the counts per pixel lie in the range of a few to a few tens of events in one ROI illustrating the impracticality of deconvolution for the specified fluorescence lines. In Fig. 3, nine pixels (3 × 3) were averaged resulting in a resolution of 537 × 495 pixels.

As reported previously, the green leaves were painted with a mixture of copper(II) carbonates (*i.e.* malachite and azurite) and lead stannate (*i.e.* lead tin yellow).[15] The related Cu and Pb distributions show two different intensity levels with the strongest signals corresponding to the leaves on the side that is facing the detector while the weaker distribution corresponds to the leaves on the *verso* side. The Sn L map shows only the leaves on the 'detector side' as the low energy of the Sn-L emission line (*ca.* 3.4–3.6 keV) is absorbed by the superimposed material on its path to the detector.

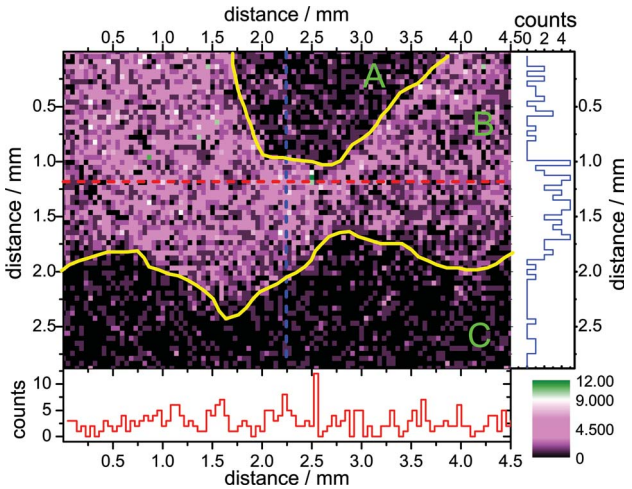

Fig. 4 Details of the Au M distribution as marked in Fig. 3 with three regions: (A) leaf paint on top of gilding, (B) gilding, (C) no gilding; the heterogeneity of the gilding thickness can be discerned directly in the lateral distribution as the fluorescence originates from the upper gold layer only.

The Pb distribution shows additionally the flowers on the detector side of the parchment. As there is no correlation with Sn, it can be assumed that lead white was used to lighten the color of the flowers. The maps suggest that the red pigment used for the flowers is most probably an organic dye (not detectable by XRF) precipitated on an inorganic Ca component (*e.g.* chalk or gypsum).

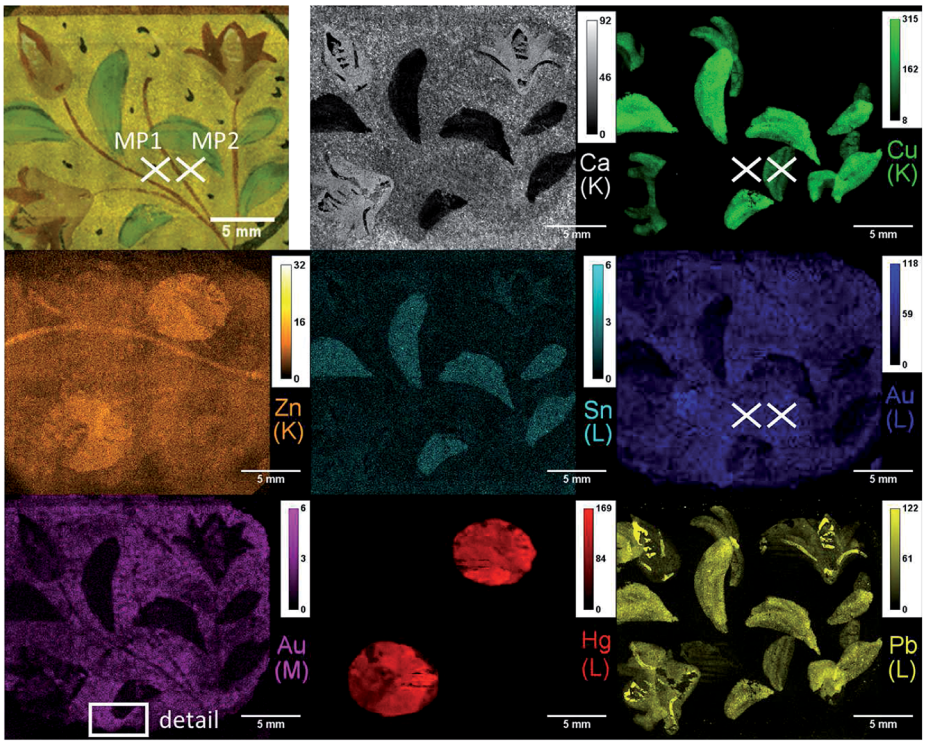

Fig. 3 Single elemental distributions resulting from the 2D-measurement; the map size is 22 × 26 mm^2, with 15 μm × 15 μm pixel size. The measurement positions (MPs) for the point spectra and confocal depth scans are indicated by a white X, while the scan area shown in Fig. 4 is indicated by a white rectangle in the Au-M distribution.

Table 1 Quantification values of the thicknesses of the Au layers at the measurement positions 1 and 2 in nanometers: values derived through the conventional micro-XRF measurements are compared to thickness values obtained through the quantification of depth profiles, conducted both from the front and the backside of the parchment. The values in brackets from the 3D measurements are only listed for the sake of completeness, not for comparison

MP		Micro-XRF	Confocal from front	Confocal from back
1	Front	105	80	(1400)
1	Back	220	(100)	450
2	Front	150	90	(40)
2	Back	40	(50)	80

In accordance with the gilding technique, the Au distribution is on the parchment as a background to the decorations. This assumption is supported by the distribution of the low energetic Au M radiation, which originates from the side facing the detector only because the radiation from the lower side is absorbed in the parchment itself. The Au M map from the 'flower' side shows the leaves and flowers as a negative, which can be understood as the absorption by the Cu and Pb pigments which are painted on top of the gilding.

When taking a closer look at the Au M map, the structure of the gilding can be examined. Fig. 4 shows a small detail of the Au M mapping with three different regions. Region C shows an area without gilding, region B the gilding and region A the gilding with the paint of a leaf on top. Although the count rate is very low, the three different regions can be distinguished and within region B, heterogeneities bigger than the statistical uncertainties can be discerned. The gilding seems worn out by long years of handling and may not be an intact layer anymore.

The Hg distribution attributed to the pigment vermillion shows two oval shapes which originate from the red colored strawberries on the reverse of the parchment. In this case, the energetic Hg-L signals (*ca.* 9.9–11.4 keV) are less attenuated and able to penetrate the overlying parchment and paint layers. An overlap of the Zn-K_α line (8.63 keV) with the Hg-Ll line (8.72 keV) and the Au-Ll line (8.49 keV) leads to an unclear Zn map. However, the stem of the strawberries can clearly be distinguished both in the Zn and Fe maps, which can be verified by examining the sum spectrum of the area.

Clearly the 2D measurement gives fast information about the lateral distribution of fluorescence elements, but depth information is uncertain at best.

The fact that the Au M radiation originates exclusively from the top layer renders a semi-quantitative analysis of the Au thickness feasible. In Fig. 3, two measurement positions are marked, where spectra with a measurement time of 120 s were additionally collected. The spectra were collected from both sides at a position where no decoration other than the gilding is present (MP1) and at a position with a green pigment on the backside (MP2). As the positioning of the sample was performed by hand, the agreement of the measurement positions (MP) from both sides is only approximate.

The Au M line intensities of these spectra were used for the determination of the thickness of the upper gold layer using a simple intensity/thickness relationship based on the Sherman equation.[8] Here, the assumption has to be made that the Au layer is homogeneous laterally and that possible depositions on

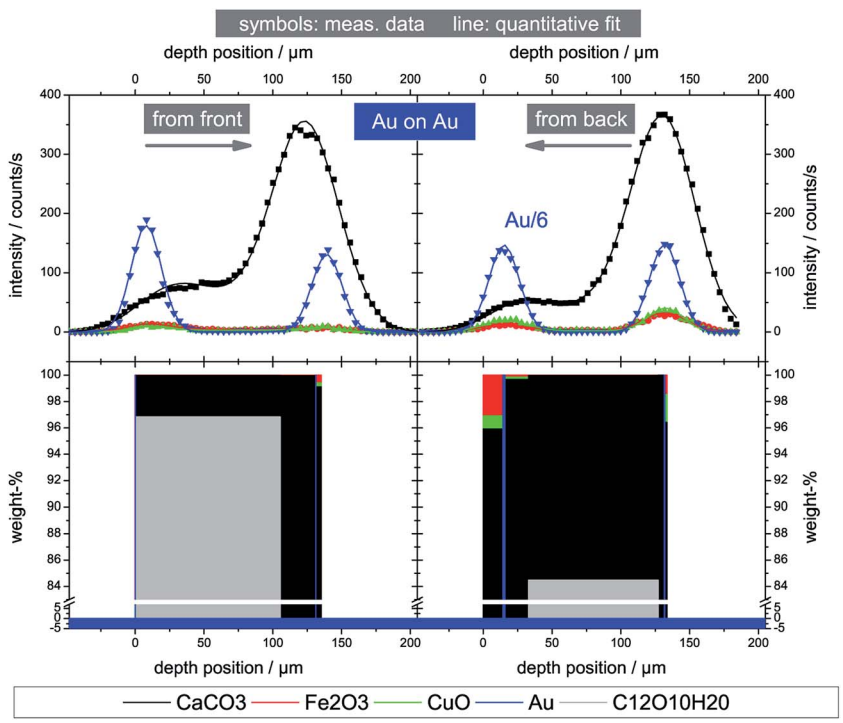

Fig. 5 Measurements on MP1: the top graphs show the Au L_α, Ca K_α, Cu K_α and Fe K_α depth profiles from the front and backside of the parchment; the bottom graphs show the reconstructed weight percent values derived by quantification. Note the down scaling of the Au profile.

top of the Au layer do not affect the quantification results presented in Table 1. The thickness values lie within 40–220 nm and show the order of magnitude. As a gold leaf is usually around 1 μm in thickness, smaller values reflect the worn out state of the gilding.

3.2 Confocal depth profiles

For a more detailed analytical examination of the layered structure, it is possible to measure confocal depth profiles at selected points and perform a semi-quantitative reconstruction of the full sample. For that purpose, single spectra were collected with a measuring time of 10 s along the *Z*-direction. With approx. 30 steps with a 10 μm step width, the complete thickness of the sample was covered. Measurements in the same positions as for the micro-XRF single spectra, MP1 and MP2 shown in Fig. 3, will be discussed in what follows. Scans were performed from both sides at approximately the same position.

The deconvolved net peak areas of the main elements as a function of depth (*Z*-position) for the two positions are displayed in the top graphs of Fig. 5 and 6. The diagrams show the measured intensities (points) and the profiles calculated with the help of a quantitative routine (lines). The zero position denotes the surface of the front side of the sample. Because of the finite size of the probing volume the layer boundaries are not sharp. Additionally, the depth resolution and the absorption of exciting and fluorescence radiation are energy and depth dependent.

For the quantification, the procedure described in detail in ref. 13 was used. The probing volume is characterized by the calibration curves of Fig. 1 and a sample model consisting of homogeneous layers must be assumed with adapted starting parameters for layer borders, densities, dark matrix composition and concentrations of the fluorescence elements. With the help of a modified Sherman equation, net peak intensities for all fluorescence lines as a function of depth are calculated simultaneously. A least squares fitting procedure then minimizes the difference between simulation and measured data.

The raw data of the measurements on MP1 from the front and the back show the same elements with similar qualitative profiles, see Fig. 5. But when comparing the intensities and considering the different absorption depending on the scan direction, quantitative differences can be identified. On the one hand, the Au L_α intensity for the two directions differs by a factor of 6. On the other hand, the Ca K_α profile suggests for the measurement from the front (top, left graph of Fig. 5) a very high amount of Ca close to the bottom layer, while the measurement from the back suggests the opposite, *i.e.* a high amount of Ca at the front surface because of the high absorption of the thicker Au layer.

The bottom graphs and Table 2 show the corresponding quantitative reconstruction of the different layers of the sample. Six to seven homogeneous layers were assumed. The parchment was defined as cellulose with a density of 1.2 g cm^{-3}, Ca is assumed to be present as chalk, Fe in the form of Fe_2O_3 and Cu as CuO as contaminants. The gold layers are metal layers with a density of 19.3 g cm^{-3}. In front of and behind the Au layers, chalk containing layers were allowed due to the preparation technique of the parchment itself or chalk residues from the gold beating. Chalk, CuO and Fe_2O_3 were allowed in all layers

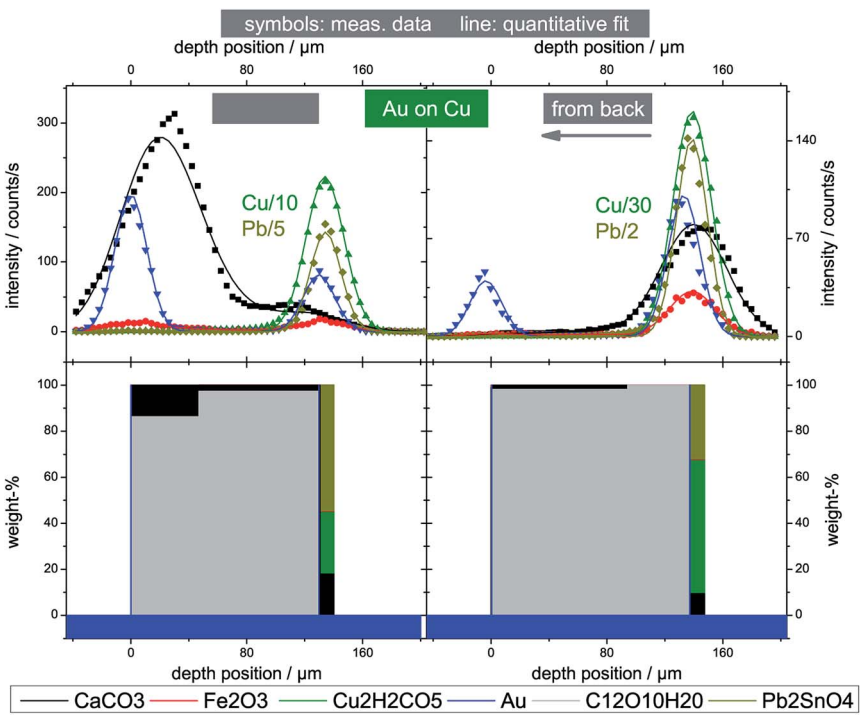

Fig. 6 Measurements on MP2: the top graphs show the Au L_α, Ca K_α, Cu K_α, Fe K_α and Pb L_α depth profiles from the front and backside of the parchment; the bottom graphs show the reconstructed weight percent values derived by quantification. Note the down scaling of the Cu and Pb profile.

Table 2 Quantitative weight percent values of the measurements on MP1 of Fig. 5

MP1	Layer	Parchment %	Chalk %	Au %	Fe_2O_3 %	CuO %	Thickness/μm	Density/g cm^{-3}
From front	Chalk	0	0	0	50	50	0.014	1.8
	Au	0	0	100	0	0	0.08	19.3
	Parchment	97	3	0	0.02	0.01	105	1.2
	Chalk	0	99.9	0	0.03	0.03	25	1.8
	Au	0	0	100	0	0	0.1	19.3
	Chalk	0	99.2	0	0.6	0.3	4	1.8
From back	Chalk	0	96	0	3	1	14	1.8
	Au	0	0	100	0	0	1.4	19.3
	Chalk	0	99.7	0	0.2	0.2	17	1.8
	Parchment	85	16	0	0.02	0.02	94	1.2
	Chalk	0	100	0	0	0	4	1.8
	Au	0	0	100	0	0	0.45	19.3
	Chalk	0	96	0	1.5	2	1.5	1.8

beside the Au layers. With fixed densities, the fit results were the concentration values and the layer thicknesses.

The fitting procedure must be adapted by hand, if the fit does not converge or yield meaningful results. For example, the fitting procedure may result in layers with zero thickness which explains the different number of layers for measurements on MP1. For the measurements of MP2 on the other hand two parchment layers were needed for a satisfactory fitting result.

As already presumed by the qualitative examination of the depth profiles, the results of the two measurements on MP1 differ strongly in their Au layer thickness and the presence of chalk containing layers.

These differences between the two measurements can be explained by two factors. On the one hand, the positions are only approximately the same. On the other hand, the layers of the parchment are laterally highly heterogeneous, see also Fig. 4. That means, when keeping in mind the 40°/40° geometry, that the absorption in the excitation and detection channel depends on the position and orientation of the sample and on the probed depth.

The measurement of MP2 with a green pigment on the backside is presented analogous to Fig. 5 in Fig. 6. In this case, for quantification the green paint was modeled as a mixture of malachite and lead-tin yellow and seven layers were assumed. The density of the paint layer was in this case used as an additional fit parameter, yielding the results displayed in the bottom graphs of Fig. 6 and Table 3. Here, the measurements are in good agreement, with a paint layer of about 10 μm thickness, Au layer thicknesses ranging from 40 nm to 90 nm and comparable elemental compositions.

All reconstructed values presented here must be regarded as semi-quantitative, as one assumption for the use of the quantification model is not strictly valid. The sample does not consist of laterally homogeneous layers. Additionally, when reconstructing six to seven layers, the uncertainties for the bottom layers increase exponentially due to the absorption dependency.

Nevertheless, when comparing the extracted thicknesses of the Au layers with the values derived from the micro-XRF quantification, see Table 1, an acceptable agreement is achieved. Additionally, the presented depth profiles show a clear separation of the top and bottom layers. With this information, parameters of the full 3D measurement of selected areas can be optimized.

3.3 3D visualization

Confocal measurements for full 3D imaging were conducted in order to image the pigment layers on the front and on the

Table 3 Quantitative weight percent values of the measurements on MP2 of Fig. 6

MP1	Layer	Parchment %	Chalk %	Au %	Fe_2O_3 %	$Cu_2H_2CO_5$ %	Pb_2SnO_4 %	Thickness/μm	Density/g cm^{-3}
From front	Chalk	0	0	0	99.9	100	0	0.01	1.8
	Au	0	0	100	0	0		0.09	19.3
	Parchment	86	14	0	0.02	0	0	47	1.2
	Parchment	97	3	0	0.01	0	0	83	1.2
	Au	0	0	100	0	0		0.05	19.3
	Chalk	0	100	0	0	0	0	0.6	1.8
	Green	0	18	0	0.23	27	55	10	6
From back	Chalk	0	99	0	1	0	0	0.4	1.8
	Au	0	0	100	0	0		0.04	19.3
	Parchment	98	2	0	0.01	0	0	94	1.2
	Parchment	99.9	0	0	0.01	0	0	43	1.2
	Au	0	0	100	0	0		0.08	19.3
	Green	0	9	0	0.3	58	32	10	2.2

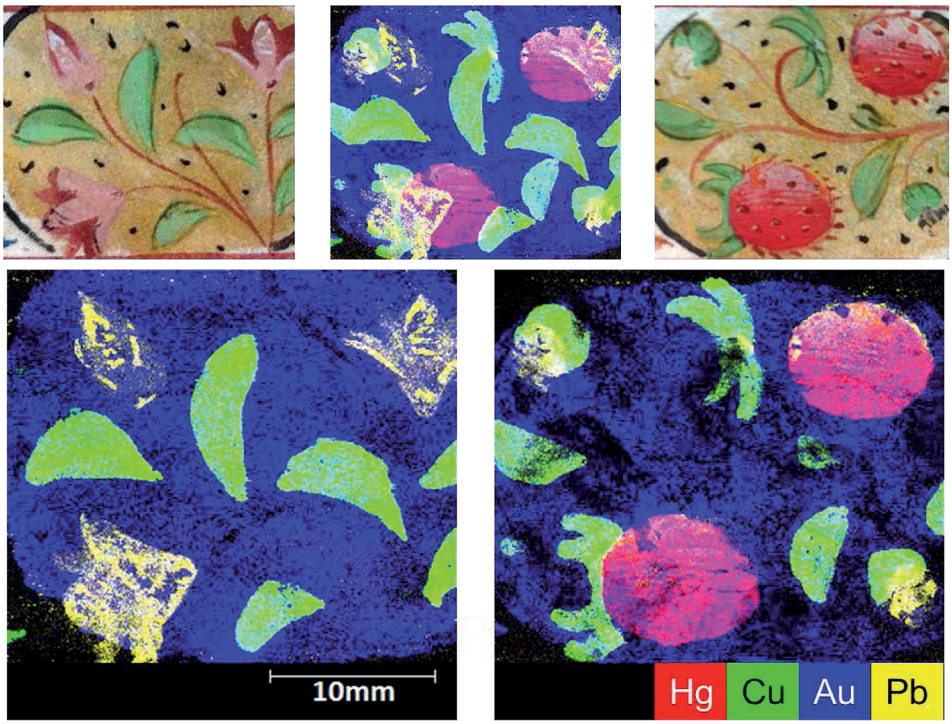

Fig. 7 3D measurement of the 'strawberry' area with Hg L_α: red, Cu K_α: green, Au L_α: blue, and Pb L_α: yellow; optical images of the scanned area (top left: backside, top right: front side); maximum intensity signals of all measured slices (top middle); separated elemental distributions of the backside (bottom left) and front side (bottom right).

backside of the parchment. The 'scrollwork' area marked in yellow in Fig. 2 was measured from the front side and the 'strawberry/flower' area marked in white from the back/flower side.

Fig. 7 shows the measurement of the 'strawberry/flower' area. Here, the lateral step size was set to 90 μm with 300 pixels × 262 pixels for the 27 mm × 23.6 mm map. Through the introduction of an additional polycapillary optic in front of the detector, the intensity during the confocal measurements is reduced compared to 2D measurements. For that reason, the pixel dwell time was prolonged to 15 ms, resulting in a measurement time per slice of 40 min. With a 15 μm step size in the direction of the sample normal and 87 slices, the total measurement time amounted to 30 hours. Every slice was saved as a so-called hypermap and exported as an 8 bit RGB picture with normalized color values (0 : 255). A video image of the front and backside of the analyzed area is shown in the top left and right figures of Fig. 7. The top middle figure of Fig. 7 shows

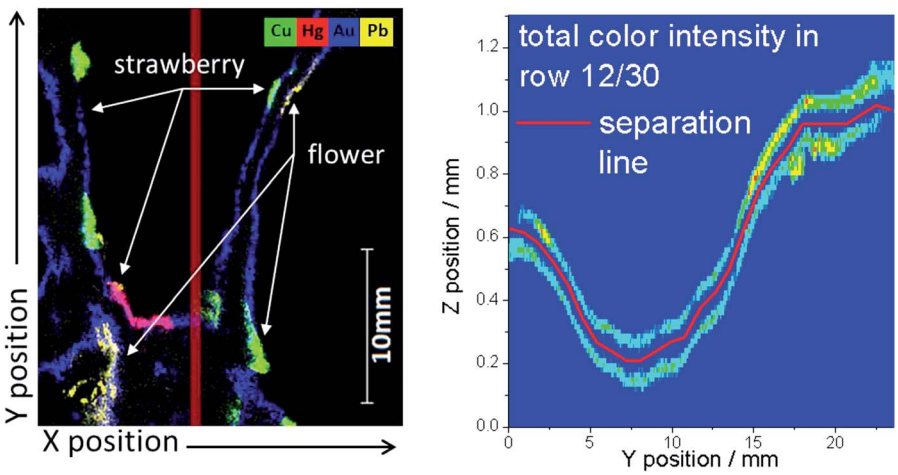

Fig. 8 Left: one slice of the 3D measurement with Hg L_α: red, Cu K_α: green, Au L_α: blue, and Pb L_α: yellow: as the parchment is not flat, displaying a wavy surface; one slice features areas stemming from both *recto* and *verso* side decorations; the images were divided into 30 vertical slices (red bar) and summed in the *X*-direction; right: resulting *ZY*-slice of the 3D-distribution with a spline (red) enabling the layer separation.

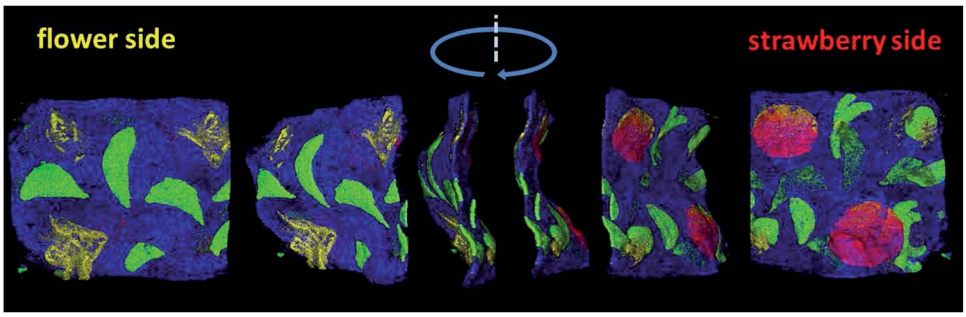

Fig. 9 Views of the composite 3D-distribution with Hg L_α: red, Cu K_α: green, Au L_α: blue, and Pb L_α: yellow; the depth axis is stretched by a factor of 10 for a better visualization.

the maximum intensity distribution for Hg (red), Au (blue), Pb (yellow) and Cu (green), derived by selecting for each lateral pixel the maximum intensity value of the respective element from all measured slices.

Fig. 8 (left) shows the respective distributions of one single slice. In this map, information from the top layer (*i.e.* 'flower' side of the parchment) and the bottom layer ('strawberry' side) is mixed, as the parchment was not completely flat. Over an area of 27 mm × 23.6 mm, the parchment's Z variation is smaller than 1.2 mm with an approximate sample thickness of $d \leq 140$ μm.

For a better understanding of the sample, a 3D representation can be generated by arranging the slices. Six views of this distribution are shown in Fig. 9 and animations are shown in the ESI.† Also these distributions show that the parchment is not flat which complicates the interpretation of the data.

For a separation of the pigment layers the dataset was further processed. The two layers were separated by a spline as shown for one vertical slice in the right part of Fig. 8. The measured maps were divided into 30 vertical slices, see the red bar in the left picture of Fig. 8, and summed in the X-direction. The summed counts were then displayed in a 2D ZY-map, see right image of Fig. 8. For all 30 slices, a spline with 23 points was defined by hand and then the data of the two parts was separated. Afterwards, maximum intensity distributions for the top and bottom part were generated resulting in a separation of both pigment layers. In the bottom graphs of Fig. 7, the results of this procedure are shown. The bottom right image was

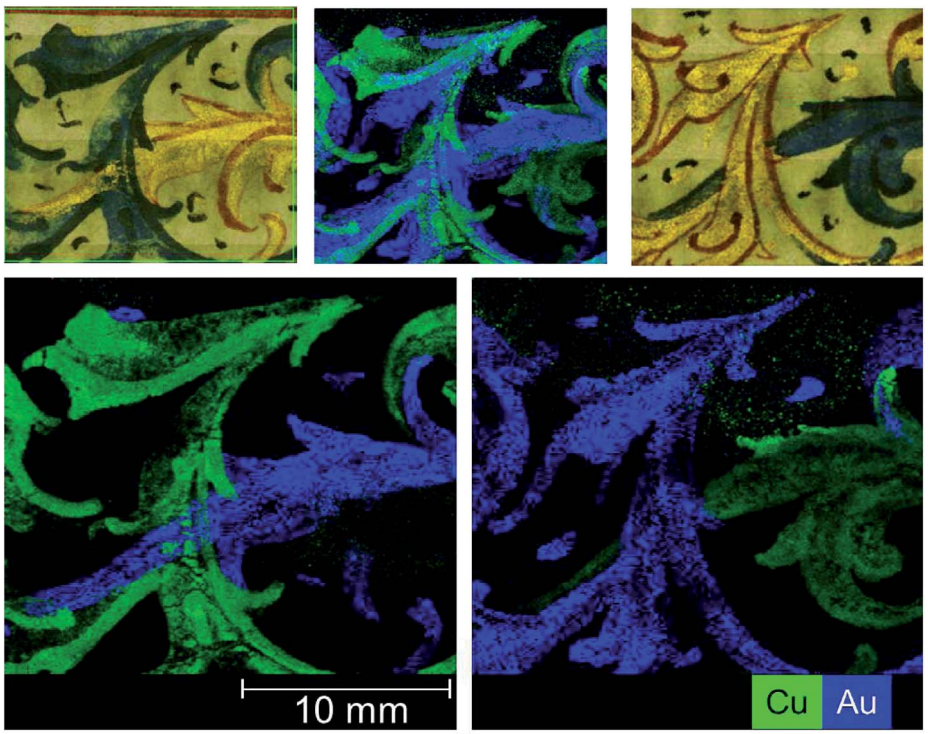

Fig. 10 3D measurement of the 'scrollwork' area with Cu K_α: green and Au L_α: blue; optical images of the scanned area (top left: backside, top right: front side); maximum intensity signals of all measured slices (top middle); separated elemental distributions of the backside (bottom left) and front side (bottom right).

mirrored in order to facilitate the comparison with the top right photograph.

The 'scrollwork' area marked in Fig. 2 with yellow was measured from the front side and the data were processed accordingly, see Fig. 10. The map consisting of 260 pixels × 228 pixels in 34 slices was measured in approximately 22 hours. In the representation, only the Cu K_α (green) and Au L_α (blue) fluorescence intensities are displayed which overlap in the 2D map.

Through the use of the maximum intensity values for each pixel, some pixels show an artificially enhanced intensity resulting in an artifact resembling background noise, see the green 'noise' in the bottom images of Fig. 6. Other than that, also in this example the two layers are completely separated making the visualization of structures painted with the same pigments possible.

4 Conclusions

We have presented the added value of both 2D and 3D micro X-ray fluorescence analysis of an illuminated, double-sided parchment sample with respect to conventional point measurements, and this by exploiting the different measurement modes of one single laboratory instrument. Fast 2D mapping enables the collection of detailed lateral information on the distribution of the main elements. By analyzing the sum spectra of specific areas, minor elements or traces can be identified which make the identification of specific pigments such as lead-tin yellow feasible. By collecting point spectra with higher measurement times, in principle layer thicknesses can be derived. When using a confocal setup, semi-quantitative values for layer composition and thickness of all layers can be extracted through a reconstruction of the measured depth profiles. This quantification with a laboratory setup is shown here for the first time for a real sample.

By using the information on the reconstruction of the depth profiles in order to optimize measurement parameters, the three-dimensional visualization of a sample becomes possible within a practical experiment time. In particular, a 3D representation of two areas on the parchment was performed with a complete separation of the decorations on the front and backside of the parchment. Besides the aforementioned noise artifact, the separation examples reflect the decoration without ambiguity.

This procedure is well suited for illuminated manuscripts, as the absorption by the organic parchment matrix is low. As a result, information can be derived from throughout the whole sample. In the presented cases, only binary information was of interest, *i.e.* if an element is present in a specific pixel or not. For the investigation of concentration differences or gradients, longer measurement times per pixel are mandatory. Only with reasonable count rate statistics can an absorption correction be performed. Nevertheless, the presented procedure enables the investigation of samples, where the backside is not accessible.

Thus, through the combination of 0D (point spectra), 1D (depth profiles), 2D and 3D analyses, an improved investigation of highly heterogeneous objects such as illuminated parchment samples is facilitated.

Acknowledgements

The authors thank Prof. Dr Birgit Kanngießer for her support and Ulrich Waldschläger and Falk Reinhardt from Bruker Nano GmbH for their fruitful cooperation.

References

1 R. J. Clark, *C. R. Chim.*, 2002, **5**, 7–20.
2 A. Adriaens, *Spectrochim. Acta, Part B*, 2005, **60**, 1503–1516.
3 D. C. Creagh and D. A. Bradley, *Radiation in Art and Archeometry*, Elsevier Science, Amsterdam and New York, 1st edn, 2000.
4 G. van der Snickt, C. Miliani, K. Janssens, B. G. Brunetti, A. Romani, F. Rosi, P. Walter, J. Castaing, W. de Nolf, L. Klaassen, I. Labarque and R. Wittermann, *J. Anal. At. Spectrom.*, 2011, **26**, 2216.
5 M. Haschke and M. Haller, *X-Ray Spectrom.*, 2003, **32**, 239–247.
6 K. Janssens, K. Proost and G. Falkenberg, *Spectrochim. Acta, Part B*, 2004, **59**, 1637–1645.
7 B. Kanngießer, W. Malzer and I. Reiche, *Nucl. Instrum. Methods Phys. Res., Sect. B*, 2003, **211**, 259–264.
8 J. Sherman, *Spectrochim. Acta*, 1955, **7**, 283–306.
9 I. Mantouvalou, W. Malzer and B. Kanngießer, *Spectrochim. Acta, Part B*, 2012, **77**, 9–18.
10 I. Mantouvalou, W. Malzer, I. Schaumann, L. Lühl, R. Dargel, C. Vogt and B. Kanngiesser, *Anal. Chem.*, 2008, **80**, 819–826.
11 D. K. G. De Boer, *X-Ray Spectrom.*, 1989, **18**, 119–129.
12 M. Mantler, *Anal. Chim. Acta*, 1986, **188**, 25–35.
13 I. Mantouvalou, T. Wolff, C. Seim, V. Stoytschew, W. Malzer and B. Kanngiesser, *Anal. Chem.*, 2014, **86**, 9774–9780.
14 M. Czyzycki, D. Wegrzynek, P. Wrobel and M. Lankosz, *X-Ray Spectrom.*, 2011, **40**, 88–95.
15 G. van der Snickt, W. de Nolf, B. Vekemans and K. Janssens, *Appl. Phys. A: Mater. Sci. Process.*, 2008, **92**, 59–68.
16 M. Haschke, U. Waldschläger, R. Tagle and U. Rossek, *Microsc. Microanal.*, 2012, **18**, 946–947.